

The role of minor alloying in the plasticity of bulk metallic glasses

Sven Hilke^a, Harald Rösner^{a,*}, Gerhard Wilde^a

^a*Institut für Materialphysik, Westfälische Wilhelms-Universität Münster, Wilhelm-Klemm-Str. 10, 48149 Münster, Germany*

Abstract

Micro- or minor alloying of metallic glasses is of technological interest since it has been shown to improve the ductility. An originally ductile Pd-based monolithic bulk metallic glass (Pd₄₀Ni₄₀P₂₀) was selectively manipulated by additions of Fe or Co. The alloying effects were extreme, showing either exceptional ductility upon Co addition or immediate catastrophic failure upon Fe addition when tested under uniaxial compression or 3-point bending. The amorphous structure was characterized prior to deformation with respect to its medium-range order (MRO) using variable resolution fluctuation electron microscopy (VR-FEM). We observe striking differences in the MRO between the ductile and brittle metallic glasses, with the ductile glasses exhibiting a rich structural diversity, which seems to enable easier shear banding and hence enhances the deformability.

Keywords: bulk metallic glass; micro-alloying; fluctuation electron microscopy; diffraction; amorphous; deformation

Bulk metallic glasses (BMGs) are promising candidates for applications [1–4]. However, most BMGs lack ductility, particularly under tension where, at the end of the elastic regime, immediate catastrophic failure predominates [5]. Progress has been made in recent years in developing monolithic BMGs exhibiting respectable ductility during cold rolling, bending or compression tests [6–14]. The key parameter for the plasticity seems to be the structural heterogeneity of the amorphous materials, which can be manipulated for example by micro- or minor alloying [7, 10, 15–19]. However, the structural heterogeneity is still an ill-defined entity although it is frequently referred to in connection with the amorphous structure of monolithic metallic glasses. Thus, understanding the amorphous structure is of importance. For this purpose, the concept of medium-range order (MRO) is used to describe structural correlations in the amorphous state having length scales between that of atomic bonding and crystalline order. Different MRO models have been proposed claiming MRO correlation lengths or sizes in the range of about 1 nm [20], 1–2 nm [21, 22], 1–3 nm [23–25], 1–4 nm [26–28] or generally larger than > 0.5 nm (short-range order) [29–34].

In this study we address the structure-property relation using a ternary Pd-based BMG (Pd₄₀Ni₄₀P₂₀), which was selectively manipulated by minor additions of Fe or Co. The glassy materials were characterized with respect to their MRO using variable resolution fluctuation electron microscopy (VR-FEM). FEM is a microscopic technique based on a statistical analysis of the variance $V(|\vec{k}|, R)$ determined from diffracted intensities of nanometer-sized

volumes obtained by scanning transmission electron microscopy (STEM) microdiffraction [28, 30, 35–37]. The advantage of FEM is that it contains information on the pair-pair correlations and hence on the MRO [28, 31, 38–40]. The normalized variance $V(|\vec{k}|, R)$ of the spatially resolved diffracted intensity I of a nanobeam diffraction pattern (NBDP) is therefore a function of the scattering vector \vec{k} and the coherent spatial resolution R :

$$V(|\vec{k}|, R) = \frac{\langle I^2(\vec{k}, R, \vec{r}) \rangle}{\langle I(\vec{k}, R, \vec{r}) \rangle^2} - 1 \quad (1)$$

where $\langle \rangle$ indicates the averaging over different sample positions \vec{r} or volumes, and R denotes the FWHM of the electron probe [32]. Sampling with different parallel coherent probe sizes, R , is called VR-FEM [41, 42]. It gives insight into the structural ordering length scale and, using either peak height or peak integral, provides a semi-quantitative measure of the MRO volume fraction. Differences in MRO sizes (strictly MRO correlation lengths) may then be compared with differences in the properties of the BMGs [31, 38, 40, 43].

Pd₄₀Ni₄₀P₂₀ samples (master alloy) were produced by melting pure ingots of Pd (99.5%) and Ni₂P (99.9%) in a melt spinner under argon atmosphere. This master alloy was subsequently manipulated by additions of 1 at.% Co or 0.6 at.% Fe. Prior to casting, the ingots were cycled with boron oxide (B₂O₃) to purify the samples. For the deformation tests samples were cut out of the ingots using a diamond wire saw to give dimensions of 4 mm (length) x 3 mm (diameter) providing a 4:3 aspect ratio [44, 45]. Uniaxial compression tests were performed in an Instron (Instron, model 1195) using a strain rate of $2.5 \times 10^{-5} \text{ s}^{-1}$. The

*Corresponding author

Email address: rosner@uni-muenster.de (Harald Rösner)

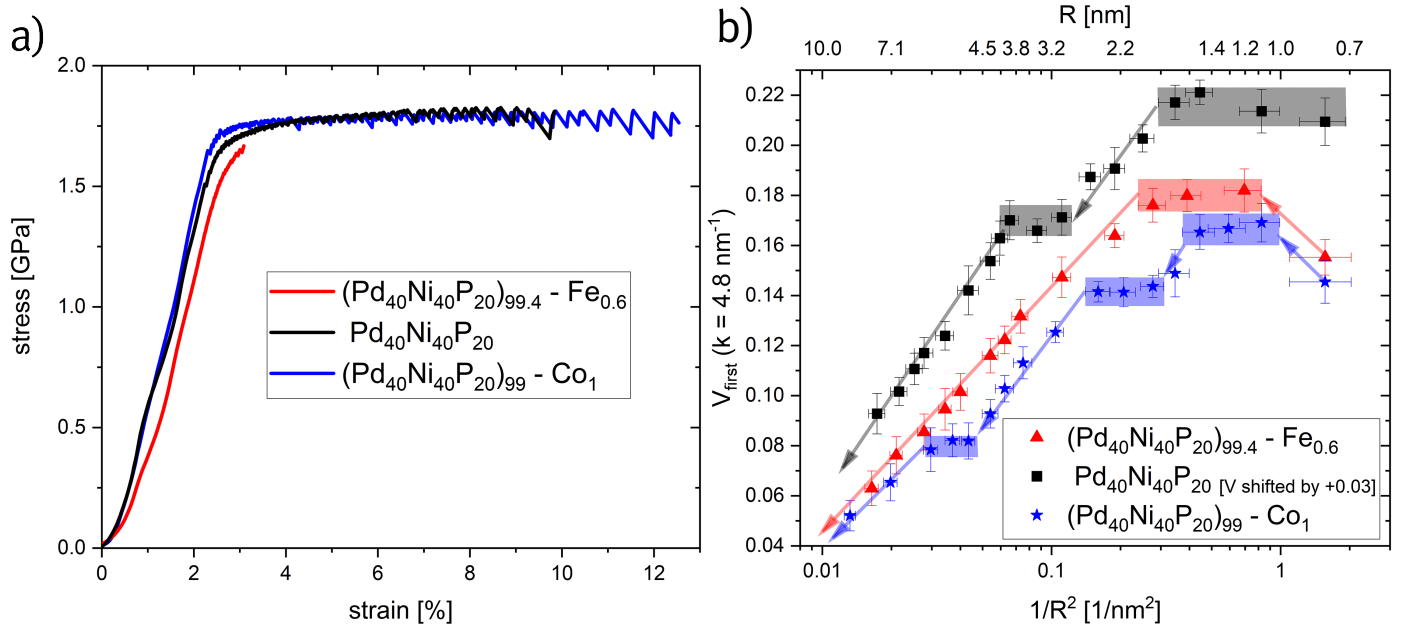


Figure 1: (a) Uniaxial compression tests of $\text{Pd}_{40}\text{Ni}_{40}\text{P}_{20}$ with additions of Fe and Co. (b) FEM analysis of the corresponding amorphous structure showing V at $k = 4.8 \text{ nm}^{-1}$ plotted against $1/R^2$. Note the difference: three plateaus for $(\text{Pd}_{40}\text{Ni}_{40}\text{P}_{20})_{99} - \text{Co}_1$ as indicated by the individual colored areas, but only one plateau for $(\text{Pd}_{40}\text{Ni}_{40}\text{P}_{20})_{99.4} - \text{Fe}_{0.6}$. For better visibility the curve of the master alloy $\text{Pd}_{40}\text{Ni}_{40}\text{P}_{20}$, showing two plateaus, has been shifted upwards (+0.03).

test device was equipped with home-made anvils of extra hardened Böhler S290 microclean steel. Since it has been demonstrated that compression tests to examine plasticity are sensitive to both alignment and shape geometry [45], 3-point bending tests were also performed. For brevity, these results are not included here but they confirmed the results of the compression tests [10, 43, 46]. More comprehensive details of the sample processing and deformation are given in reference [10]. Electron-transparent samples were prepared by electropolishing with a BK-2 electrolyte [47] at 16.5 V / -20°C using a Tenupol 5 electropolishing device (Struers A/S, Denmark).

VR-FEM was performed at 300 kV in a Thermo Fisher Scientific Themis 300 G3 transmission electron microscope (TEM). NBDPs were acquired with parallel coherent probe sizes between 0.8 and 8.5 nm at FWHM using a $10 \mu\text{m}$ C2 aperture. The probe current was set to 15 pA. The relative foil thickness (t/λ) of the TEM samples was determined by the log-ratio method using the low-loss part of electron energy loss (EEL) spectra [48]. All FEM data presented here were recorded under similar experimental conditions; that is, t/λ , beam current and acquisition time were similar in order to be sensitive to changes in the MRO measured by the normalized variance signal (peak height and shape). The dwell-time was 4 s for the individual NBDPs acquired with a CCD camera (US 2000) at binning 4 (512x512 pixels). The camera length used was 77 mm. All probe sizes were measured prior to the FEM experiments directly on the Ceta camera using Digital Micrograph plugins by D. Mitchell [49]. FEM analyses were performed on the diffracted intensities $I(\vec{k}, R, \vec{r})$ of sets of

100 individual NBDPs taken from the same scanned areas. The normalized variance profiles were calculated using a pixel by pixel analysis according to the annular mean of variance image ($\Omega_{VImage}(k)$) [50–52]. The obtained data (normalized variance profiles) is shown in the Supplementary Material (see Figs. S1-S3).

Results from previous deformation tests [10] are revisited and shown in Fig. 1a. The $\text{Pd}_{40}\text{Ni}_{40}\text{P}_{20}$ master alloy itself shows a remarkable ductility of about 8% plastic strain. A plastic strain to failure of about 10% was achieved with Co addition (1 at. %), while Fe addition (0.6 at. %) led to failure shortly after reaching the elastic limit. A compilation recording averaged results from several individual compression tests is given in Tab. 1.

In the following, our main focus is laid on the glassy structure in order to elucidate factors governing the deformation behavior of metallic glasses. “Classical diffraction” analysis (X-ray diffraction or selected area electron diffraction (SAED)) confirmed the amorphous nature of the glasses and revealed no difference between the investigated materials that would explain the large difference in deformability (see Fig. S4 and reference [10]). The results of the FEM analyses are displayed in Fig. 1b in the form of Stratton-Voyles plots [54], in which the peak intensity of the first normalized variance peak $V(k)$ at $k = 4.8 \text{ nm}^{-1}$ is plotted against $1/R^2$. As expected, one sees a general decrease of $V(k)$ as R increases. Superimposed on this are peaks or plateaus occurring when the probe size matches MRO correlation lengths present as a high volume fraction. The less well defined the MRO correlation length, the wider the plateau. The ranges of the plateaus were determined

Table 1: Tabulated data showing the discrete MRO sizes in comparison with strain to failure values (averaged) from individual uniaxial compression tests [53].

Sample	(Pd ₄₀ Ni ₄₀ P ₂₀) _{99.4} -Fe _{0.6}	Pd ₄₀ Ni ₄₀ P ₂₀	(Pd ₄₀ Ni ₄₀ P ₂₀) ₉₉ -Co ₁
MRO correlation length(s) [nm]	(1.6 ± 0.5)	(1.3 ± 0.6) (3.5 ± 0.6)	(1.3 ± 0.3) (2.2 ± 0.5) (5.3 ± 0.7)
Maximum plastic strain from compression tests [%]	(1.3 ± 0.4) averaged over 6 samples	(5.4 ± 1.6) averaged over 6 samples	(7.3 ± 2.0) averaged over 5 samples

using the individual data points including their error bars to calculate an arithmetic mean (maximum and minimum values) and these are indicated by the colored boxes in Fig. 1b. The curve of the (PdNiP)-Fe alloy exhibits a single plateau in Fig. 1b, yielding an average MRO correlation length of (1.6 ± 0.5) nm. The Stratton-Voyles plot for the very ductile (PdNiP)-Co sample, however, shows three distinct plateaus indicating a much more diverse MRO distribution with the following MRO correlation lengths: (1.3 ± 0.3) nm, (2.2 ± 0.5) nm and (5.3 ± 0.7) nm. The PdNiP ternary master alloy displays two distinct plateaus at (1.3 ± 0.6) nm and (3.5 ± 0.6) nm. These results were confirmed by further data sets taken from different regions in the three samples. Thus, a pronounced heterogeneity in terms of multiple and larger MRO correlation lengths (plateaus) was observed for the ductile materials which was not present in the brittle material. All plateau values of the FEM analysis are listed in Tab. 1.

In the following we critically review these results.

First of all, we address the observation of MRO correlation lengths extending up to 5 nm and their interpretation. Our understanding of MRO is that it describes ordering in terms of a correlation of subcritical nuclei or structural motifs present in the glassy solid at length scales beyond the first neighbor (short-range order) in the absence of long-range order (crystal). MRO manifests itself in the form of speckles in the diffraction pattern originating from such correlated structural motifs [38, 42]. Since the inspection of the individual NBDPs (~ 6000 in total) revealed only speckle contrast and no diffraction spots (reflections), we exclude the presence of crystalline fractions in the form of distinct nanocrystals for the investigated materials. The remaining question is the interpretation of the lateral extension of the observed MRO features. Our interpretation according to the Stratton-Voyles model [55] is that the spatial correlations are related to connected clusters of topologically crystalline atoms [34, 56]. This defines paracrystalline grains embedded in glassy materials representing the seeds (precursors) for crystallization. A former high-resolution TEM study using an aberration corrector for direct imaging reported extended MRO regions with a diameter of 2.5 nm for Pd₄₀Ni₄₀P₂₀ supports our interpretation of paracrystalline grains [57]. However, the focus of this study is laid on the novelty that the MRO correlation lengths (sizes) extend up to 5 nm. MRO shapes,

types, volume fractions or orientational correlations are of interest [58] but beyond the scope of this letter.

Next, we address the question how the MRO relates to the plasticity of BMGs. Upon inhomogeneous deformation, that is in our case at low temperatures and high stresses, metallic glasses exhibit plasticity in the form of a macroscopic sliding along localized regions called shear bands having thicknesses of about 15 nm or less [59–61]. The deformed samples which were ductile revealed a high number of finely dispersed shear bands penetrating through the surfaces [62], while the brittle Fe-doped material developed only a few shear bands of which one of them led to catastrophic failure [10, 62]. Thus, the plasticity of metallic glasses is based upon their ability to form multiple shear bands [63]. Our observations strongly suggest that the ductility is related to the structural heterogeneity in terms of the diversity of MRO enabling easier shear banding (see Fig. 1b).

The MRO diversity is also in accordance with models of geometrically unfavored motifs (GUMs) [64, 65] or flexibility volume [66], where mixtures of geometrically favored and unfavored motifs impart more flexibility to facilitate plastic events. Interestingly, our finding also explains an improved ductility of BMGs achieved by elastic cycling [19] since this process shuffles the atoms/clusters subsequently leading to extended MRO.

Finally, it is worth noting that the Poisson’s ratio of the three BMGs investigated (here $\nu = 0.4$) remained unaffected by the minor alloying [10]. Thus, an explanation based on the relatively high Poisson’s ratio as a factor for good deformability can be excluded here [67].

In conclusion: While ”classical diffraction“ (X-ray diffraction or selected area electron diffraction) revealed no difference that explains the difference in deformability, our data obtained by VR-FEM present clear evidence that minor alloying has a huge impact on the correlation of the glassy structures beyond the typically reported 2 nm range, which directly affects the ductility of the material. This, in turn, makes minor alloying very promising for tuning the properties of metallic glasses via MRO engineering.

Acknowledgements

We gratefully acknowledge financial support by the DFG via WI 1899/29-1 (project number 325408982). The

DFG is further acknowledged for funding our TEM equipment via the Major Research Instrumentation Program under INST 211/719-1 FUGG. We are also indebted to A. Hassanpour, Drs V. Hieronymus-Schmidt and N. Nollmann for TEM sample preparation and deformation tests, respectively.

References

- [1] J. Schroers, *Advanced Materials* 22 (2010) 1566–1597.
- [2] J. Schroers, T. M. Hodges, G. Kumar, H. Raman, A. J. Barnes, Q. Pham, T. A. Waniuk, *Materials Today* 14 (2011) 14–19.
- [3] J. Schroers, *Physics Today* 66 (2013) 32.
- [4] M. A. Gibson, N. M. Mykulowycz, J. Shim, R. Fontana, P. Schmitt, A. Roberts, J. Ketkaew, L. Shao, W. Chen, P. Bordenithikasem, J. S. Myerberg, R. Fulop, M. D. Verminski, E. M. Sachs, Y.-M. Chiang, C. A. Schuh, A. J. Hart, J. Schroers, *Materials Today* 21 (2018) 697–702.
- [5] M. F. Ashby, A. L. Greer, *Scripta Materialia* 54 (2006) 321–326.
- [6] C. A. Schuh, T. C. Hufnagel, U. Ramamurty, *Acta Materialia* 55 (2007) 4067–4109.
- [7] J. Eckert, J. Das, S. Pauly, C. Duhamel, *J. of Materials Research* 22 (2007) 285–301.
- [8] S. Scudino, B. Jerliu, S. Pauly, K. B. Surreddi, U. Kühn, J. Eckert, *Scripta Materialia* 65 (2011) 815–818.
- [9] I. V. Okulov, I. V. Soldatov, M. F. Sarmanova, I. Kaban, T. Gemming, K. Edström, J. Eckert, *Nat. Commun.* 6 (2015) 1–6.
- [10] N. Nollmann, I. Binkowski, V. Schmidt, H. Rösner, G. Wilde, *Scripta Materialia* 111 (2016) 119–122.
- [11] S. Scudino, J. J. Bian, H. S. Shahabi, D. Şopu, J. Sort, J. Eckert, G. Liu, *Scientific Reports* 8 (2018) 1–12.
- [12] X. L. Bian, D. Zhao, J. T. Kim, D. Şopu, G. Wang, R. Pippan, J. Eckert, *Mater. Science and Engineering: A* 752 (2019) 36–42.
- [13] C. X. Peng, D. Şopu, Y. Cheng, K. K. Song, S. H. Wang, J. Eckert, L. Wang, *Materials & Design* 168 (2019) 107662.
- [14] K. Kosiba, D. Şopu, S. Scudino, L. Zhang, J. Bednarcik, S. Pauly, *J. of Plasticity* 119 (2019) 156–170.
- [15] X. Wang, Q. P. Cao, Y. M. Chen, K. Hono, C. Zhong, Q. K. Jiang, X. P. Nie, L. Y. Chen, X. D. Wang, J. Z. Jiang, *Acta Materialia* 59 (2011) 1037–1047.
- [16] G. Q. Guo, L. Yang, *Intermetallics* 65 (2015) 66–74.
- [17] N. C. Wu, L. Zuo, J. Q. Wang, E. Ma, *Acta Materialia* 108 (2016) 143–151.
- [18] R. Hubek, M. Seleznev, I. Binkowski, M. Peterlechner, S. V. Divinski, G. Wilde, *J. of Appl. Phys.* 124 (2018) 225103.
- [19] S. Im, P. Zhao, G. H. Yoo, Z. Chen, G. Calderon, M. A. Gharacheh, O. Licata, B. Mazumder, D. A. Muller, E. S. Park, Y. Wang, J. Hwang, *arXiv preprint arXiv:2002.09347* (2020).
- [20] R. K. Dash, P. M. Voyles, J. M. Gibson, M. M. J. Treacy, P. Keblinski, *J. of Physics: Condensed Mat.* 15 (2003) S2425.
- [21] J. M. Gibson, M. M. J. Treacy, T. Sun, N. J. Zaluzec, *Phys. Rev. Lett.* 105 (2010) 125504.
- [22] X. Zhan, P. Zhang, P. M. Voyles, X. Liu, R. Akolkar, F. Ernst, *Acta Materialia* 122 (2017) 400–411.
- [23] S. N. Bogle, P. M. Voyles, S. V. Khare, J. R. Abelson, *J. of Physics: Condensed Mat.* 19 (2007) 455204.
- [24] K. B. Borisenko, B. Haberl, A. C. Y. Liu, Y. Chen, G. Li, J. S. Williams, J. E. Bradby, D. J. H. Cockayne, M. M. J. Treacy, *Acta Materialia* 60 (2012) 359–375.
- [25] J. M. Cowley, *Ultramicroscopy* 90 (2002) 197–206.
- [26] S. N. Bogle, L. N. Nittala, R. D. Twisten, P. M. Voyles, J. R. Abelson, *Ultramicroscopy* 110 (2010) 1273–1278.
- [27] B.-S. Lee, G. W. Burr, R. M. Shelby, S. Raoux, C. T. Rettner, S. N. Bogle, K. Darmawikarta, S. G. Bishop, J. R. Abelson, *Science* 326 (2009) 980–984.
- [28] P. M. Voyles, D. A. Muller, *Ultramicroscopy* 93 (2002) 147–159.
- [29] P. Biswas, R. Atta-Fynn, S. Chakraborty, D. A. Drabold, *J. of Physics: Condensed Matter* 19 (2007) 455202.
- [30] P. M. Voyles, J. M. Gibson, M. M. J. Treacy, *Microscopy* 49 (2000) 259–266.
- [31] P. M. Voyles, J. Hwang, *Fluctuation Electron Microscopy*, American Cancer Society, 2012, pp. 1–7.
- [32] F. Yi, P. Tiemeijer, P. M. Voyles, *J. of Electron Microscopy* 59 (2010) S15–S21.
- [33] P. Zhang, J. J. Maldonis, M. F. Besser, M. J. Kramer, P. M. Voyles, *Acta Materialia* 109 (2016) 103–114.
- [34] P. Zhang, Z. Wang, J. H. Perepezko, P. M. Voyles, *J. of Non-Crys. Solids* 491 (2018) 133–140.
- [35] T. Iwai, P. M. Voyles, J. M. Gibson, Y. Oono, *Phys. Rev. B* 60 (1999) 191.
- [36] P. M. Voyles, M. M. J. Treacy, J. M. Gibson, H. C. Jin, J. R. Abelson, *MRS Online Proceedings Library Archive* 589 (1999).
- [37] F. Yi, P. M. Voyles, *Ultramicroscopy* 111 (2011) 1375–1380.
- [38] M. M. J. Treacy, J. M. Gibson, *Acta Crystallographica Section A: Foundations of Crystallography* 52 (1996) 212–220.
- [39] M. M. J. Treacy, J. M. Gibson, L. Fan, D. J. Paterson, I. McNulty, *Reports on Progress in Physics* 68 (2005) 2899.
- [40] J. Hwang, P. M. Voyles, *Microsc. Microanal.* 17 (2011) 67–74.
- [41] M. M. J. Treacy, D. Kumar, A. Rougee, G. Zhao, P. R. Buseck, I. McNulty, L. Fan, C. Rau, J. M. Gibson, *J. of Phys.: Condensed Mat.* 19 (2007) 455201.
- [42] M. M. J. Treacy, *Ultramicroscopy* 107 (2007) 166–171.
- [43] F. A. Davani, S. Hilke, H. Rösner, D. Geissler, A. Gebert, G. Wilde, *arXiv preprint arXiv:2003.01368* (2020).
- [44] R. D. Conner, W. L. Johnson, N. E. Paton, W. D. Nix, *J. of Appl. Phys.* 94 (2003) 904–911.
- [45] W. F. Wu, Y. Li, C. A. Schuh, *Phil. Mag.* 88 (2008) 71–89.
- [46] F. A. Davani, S. Hilke, H. Rösner, D. Geissler, A. Gebert, G. Wilde, *J. of Alloys and Compounds* (2020). In print.
- [47] B. J. Kestel, *Ultramicroscopy* 19 (1986) 205–211.
- [48] T. Malis, S. C. Cheng, R. F. Egerton, *J. of Electron Microscopy Technique* 8 (1988) 193–200.
- [49] D. R. G. Mitchell, B. Schaffer, *Ultramicroscopy* 103 (2005) 319–332.
- [50] T. L. Daulton, K. S. Bondi, K. F. Kelton, *Ultramicroscopy* 110 (2010) 1279–1289.
- [51] V. Schmidt, H. Rösner, M. Peterlechner, G. Wilde, P. M. Voyles, *Phys. Rev. Lett.* 115 (2015) 035501.
- [52] C. Gammer, C. Mangler, C. Rentenberger, H. P. Karthaler, *Scripta Materialia* 63 (2010) 312–315.
- [53] N. Nollmann, *Plastische Deformation und mechanische Eigenschaften von Palladium-basierten metallischen Glasern*, Ph.D. thesis, Westfälische Wilhelms Universität Münster, 2018.
- [54] W. G. Stratton, P. M. Voyles, *Ultramicroscopy* 108 (2008) 727–736.
- [55] W. G. Stratton, P. M. Voyles, *J. of Physics: Cond. Matter* 19 (2007) 455203.
- [56] D. Ma, A. D. Stoica, X.-L. Wang, *Nature Materials* 8 (2009) 30–34.
- [57] A. Hirata, Y. Hirotsu, T. Nieh, T. Ohkubo, N. Tanaka, *Ultramicroscopy* 107 (2007) 116–123.
- [58] S. Im, Z. Chen, J. M. Johnson, P. Zhao, G. H. Yoo, E. S. Park, Y. Wang, D. A. Muller, J. Hwang, *Ultramicroscopy* 195 (2018) 189–193.
- [59] P. E. Donovan, W. M. Stobbs, *Acta Metallurgica* 29 (1981) 1419–1436.
- [60] V. Hieronymus-Schmidt, H. Rösner, G. Wilde, A. Zaccone, *Phys. Rev. B* 95 (2017) 134111.
- [61] S. Hilke, H. Rösner, D. Geissler, A. Gebert, M. Peterlechner, G. Wilde, *Acta Materialia* 171 (2019) 275–281.
- [62] R. Hubek, M. Seleznev, I. Binkowski, M. Peterlechner, S. V. Divinski, G. Wilde, *J. of Appl. Phys.* 127 (2020) 115109.
- [63] J. Schroers, W. L. Johnson, *Phys. Rev. Lett.* 93 (2004) 255506.
- [64] E. Ma, *Nature Materials* 14 (2015) 547.
- [65] E. Ma, J. Ding, *Materials Today* 19 (2016) 568–579.
- [66] J. Ding, Y.-Q. Cheng, H. Sheng, M. Asta, R. O. Ritchie, E. Ma, *Nat. Commun.* 7 (2016) 1–10.
- [67] J. J. Lewandowski, W. H. Wang, A. L. Greer, *Phil. Mag. Lett.* 85 (2005) 77–87.